A complete explanation of the plasmonic colours of gold nanoparticles and of the bichromatic effect

Olivier Pluchery, Yoann Prado, William Watkins

Published in J. Mater. Chem. C, 2023, 11, 15824
https://doi.org/10.1039/D3TC02669H

ARTICLE Journal of Materials Chemistry C

A Complete Explanation of the Plasmonic Colours of Gold Nanoparticles and of the Bichromatic Effect

Received 27th July 2023,
Accepted 29th September 2023

DOI: 10.1039/d3tc02669h

Olivier Pluchery,*[a] Yoann Prado [a] and William Watkins †[a]

Gold nanoparticles (AuNPS) are known for their ruby-red colour related to their localized plasmon resonance and could be used for creating a new type of colour pigments. Moreover, the colour varies if the nanoparticle suspension is observed in transmission or in diffuse reflection. We have systemetically studied this two-colour effect, called bichromatic effects for twelve samples of nanoparticles in water with increasing diameters from 16 to 108 nm. The transmission and diffuse reflection spectra were recorded and compared to an analytical model based on the scattering cross sections calculated with the Mie theory. We have also calculated and represented the colours within the CIE colour diagram. This approach provides a very efficient way for predicting the colouring power of plasmonic pigments when AuNPs are embedded in a material. It stresses that spherical gold nanoaprticles may exhibit a nice bichromatic effect when their diameter is between 70 and 90 nm.

Introduction

The ruby-red colour of gold nanoparticles (AuNPs) is a vivid illustration on how optical properties of metals are transformed when their size is reduced to nanometer dimensions.[1, 2] In the case of gold, a suspension of nanoparticles of diameters between 10 and 50 nm displays a red colour in transmission which is related to the fact that it absorbs strongly in the green. The initial light then appears with a deficit of green and is therefore perceived as red by the observer, as expected for subtractive colour mixing. For AuNPs suspensions, the green absorption is caused by the localized plasmon resonance (LSPR) at 520 nm excited by the incoming light.[3, 4] This class of colours is called plasmonic colours[5], and is based on a mechanism of light-matter interaction that differs from that of the dyes which is also known as chemical colour and represents the vast majority of the visible colours in nature. It also differs from the structural colours that are physical colours based on interferometric mechanisms.

The emblematic example of plasmonic colours is certainly the Lycurgus cup which appears with two different colours, depending if the illumination is placed on the observer side, or across the cup: in the first case the colour is green and is controlled by the scattering by nanoparticles. In the second case, the colour is red, and is set by the wavelengths absorbed by the nanoparticles.[6] It was shown that the glass of this cup contained 70 nm gold-silver alloyed nanoparticles. [7, 8] It is established that this dual colour effect which is also termed bichromatic or dichroic effect, results from a competition between the ability of plasmonics nanoparticles to absorb light preferentially at the LSPR wavelength, and their ability to scatter at this wavelength. When scattering dominates the LSPR colour is observed and when absorption dominates, the complementary colour is seen. The wavelength of the absorption peak and the wavelength of the scattering peak are usually almost identical, so that the colours in transmission and in diffusion are complementary colours. Also notice that most of the publications about plasmonic colours deal with the absorption of light at LSPR wavelengths since scattering is usually negligible.[3]

The ruby-red appearance of gold nanoparticles assemblies that are observed in transparency can be precisely related to the size, the shape and the concentration of the nanoparticles, through the calculation of extinction cross section of a single particle.[9] Calculations are able to reproduce the absorption spectra with a good accuracy, using either the analytical model of the Mie theory in case of nanospheres, or other numerical approaches such as the discrete dipole approximation (DDA) for more complex nanoparticle shapes.[10, 11] The colour observed in transparency can be predicted, after calculating the transmission spectra.[12] It has opened new opportunities for using plasmonic particles as pigments[13, 14] or anticounterfeiting processes.[15] The enhanced possibilities of plasmonic colours have actually attracted much attention recently developing the applications from metasurfaces with various lithographic plasmonic nanostructures on surfaces.[5, 16-19] A patent was filed on the process of producing bichromatic materials.[20]

The developments are much more limited for plasmonic colours observed in diffusion or reflectance. Qualitatively, it is easy to understand that these colours will be mostly controlled by the scattering cross section of the nanoparticles. The scattering of plasmonic surfaces or metasurfaces have been addressed.[16, 21] However, in the literature, and to our knowledge, there is no example of prediction and calculation of the diffused spectra of plasmonic bulk materials. Scattering cross sections of individual

[a] Institut des NanoScience de Paris, Sorbonne University, CNRS, UMR7588, 4 place Jussieu, 75005, Paris, France
† present address: HORIBA Europe Research Center, 14 Boulevard Thomas Gobert, 91120 Palaiseau, France.

Electronic Supplementary Information (ESI) available: TEM images, calculated optical cross sections for all twelve samples, calculated and measured spectra for all samples, detailed derivation of the analytical formula, snapshot of the web interface developed for this study, tables with colour coordinates for all samples. See DOI: 10.1039/x0xx00000x

Published in J. Mater. Chem. C, 2023, 11, 15824
https://doi.org/10.1039/D3TC02669H

plasmonic nanostructures were calculated but, the colour of a bulk material containing such nanostructures was not addressed. Using nanoparticle-based materials for designing plasmonic is very promising and needs solid foundations for convincing the printing industry to adopt this new technology.

Here, we prepare a set of twelve suspensions containing spherical gold nanoparticles of increasing diameters between 16 and 110 nm. We measured the transmission and diffusion spectra of these colloidal solutions and we show that by correctly using the Mie theory, it is possible to accurately reproduce both the experimental spectra in transmission and in diffuse reflection. This opens the way for a precise calculation of the colours of plasmonic solutions or plasmonic solid materials. It also provides with an exact explanation of the bichromatic effect.

Experimental

Nanoparticle synthesis

Materials. Hydrogen tetrachloroaurate(III) hydrate ($HAuCl_4.xH_2O$, Sigma-Aldrich, 50% Au basis), Sodium citrate dihydrate (SC, Fluka, > 99.0%) were used as received. Deionized water (18 MΩ) was used in all experiments. Glassware was clean with *aqua regia*, then repeatedly rinsed with demineralized water, and let in water bath overnight. *Caution: Aqua regia is highly toxic and corrosive; it requires personal protective equipment and should be handled under a fume hood*.

AuNPs seed synthesis. AuNPs seeds **Au16** were synthesized following a modified Turkevich-Frens protocol.[22] In a 100 mL three neck flask, equipped with a condenser and a thermometer, 492 µl of a 25 mM $HAuCl_4$ aqueous solution (0.0123 mmol) diluted with 56 mL of milliQ water was heated with a heating plate. When the solution started boiling, 200 µl of sodium citrate (0.068 mmol, 20 mg) was injected under vigorous stirring. The molar ratio of citrate over gold was equal to 5 in this solution. The solution slowly turned to light purple then deep red. After 30 min, the temperature was decreased to 90°C.

AuNPs growth synthesis. This synthesis was adapted from Bastus[23] with a slight modification concerning the nature of the seeds we have used. Bastus used a reverse Turkevich methods for generating the seeds of 13.5 nm.[23]. In the same vessel, containing 28 mL of the seed solution maintained at 90°C, the solution **Au24** was prepared by two consecutive injections of 250 µL of a 25 mM HAuCl4 solution (0.00625 mmol), at intervals of 30 min. 30 min after the second injection, 10 mL of this solution was extracted and conserved as the solution **Au24**. It was replaced with 10 mL of a 3 mM solution of sodium citrate (0.03 mmol, 9 mg) in order to proceed to the next growth. The reiteration of this sequence, using the precedent solution as seeds, leads to samples **Au36**, **Au44**, **Au47**, **Au52**, **Au60**, **Au66**, **Au78**, **Au85**, **Au96**, **Au108**.

Two photographs of the solutions are shown in Figure 1. When the light source was placed behind the flasks (transmission colour, see Figure 1-a), the solutions are seen with a variation of colour from red to purple as the size increases. However, when the source of light is on the same side as the observer (diffusion color, see Figure 1-b), the photograph highlights the scattering of the light by the nanoparticles and the solution exhibits a brown-orange milky colour. The effect is clearly visible from sample **Au47** and develops further toward the larger nanoparticles size.

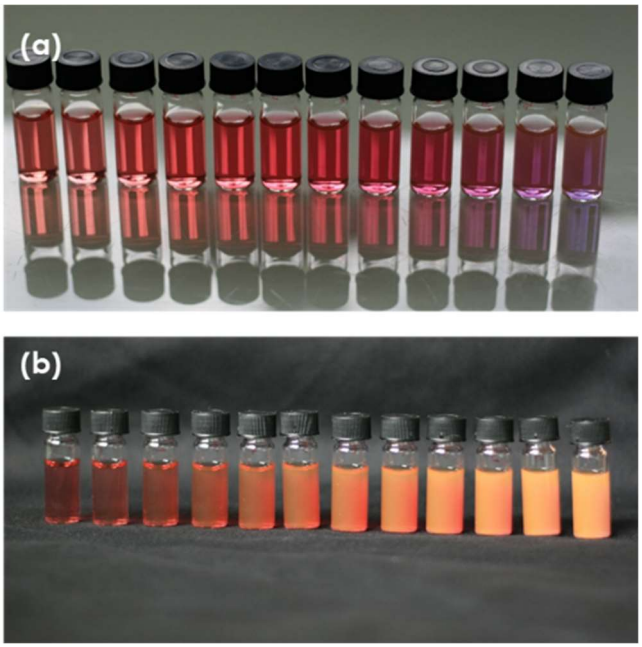

Figure 1. Photographs (a) in transmission and (b) in reflection of the twelve AuNPs dispersions of this study. The samples are named after the diameter of the nanoparticles (in nanometer), respectively from left to right: **Au16**, **Au24**, **Au36**, **Au44**, **Au47**, **Au52**, **Au60**, **Au66**, **Au78**, **Au85**, **Au96** and **Au108**.

UV-visible spectroscopy.

UV-visible spectra were recorded with a Carry 5000 spectrophotometer (Agilent) between 400 and 900 nm. A quartz cuvette from Hellma Analytics (QS high precision cell 100-10-40) with a 10 mm light path was used. Spectra were recorded for every solution in two configurations (see Figure 2): in the transmission mode and in the diffuse reflectance mode. In transmission, the cuvette was placed on the optical path of the light beam in the sample compartment of the spectrometer as shown in Figure 2-a. The values of $T = I_T/I_0$ as a function of the wavelength between 400 and 900 nm were recorded. Baselines were systematically recorded with the cuvette filled with deionized water. The diffuse reflectance spectra were acquired with an integrating sphere (Agilent, External DRA, 110 mm diameter) as depicted in Figure 2-b. The measurement mode "diffusion only" was used, in which the specular reflection I_R generated at the sample is reflected out of the integrating sphere and not integrated into the diffuse intensity I_D collected by the detector. More precisely this small opening through which the specular beam is extracted, corresponds to 3% of the total internal area of the sphere. The *dark* spectrum I_{dark} was acquired by removing the cuvette from the sample holder so

Published in J. Mater. Chem. C, 2023, 11, 15824
https://doi.org/10.1039/D3TC02669H

that no light was reflected or scattered. The 100 % reflectance signal was recorded by replacing the cuvette with a calibration standard (Spectralon, Labsphere) that diffuses more than 99% of the light back into the integrating sphere. This intensity I_0 corresponds to the spectral power of the light sources (halogen lamp for the visible and deuterium lamp for UV). The diffuse reflectance signal was computed according to: $R = 100 \times (I_D - I_{dark})/(I_0 - I_{dark})$. In this configuration, the diffuse reflectance spectra correspond to the light that is back-scattered by the cuvette in all the directions over a solid angle of 2π steradian with the exclusion of the specular reflected energy.

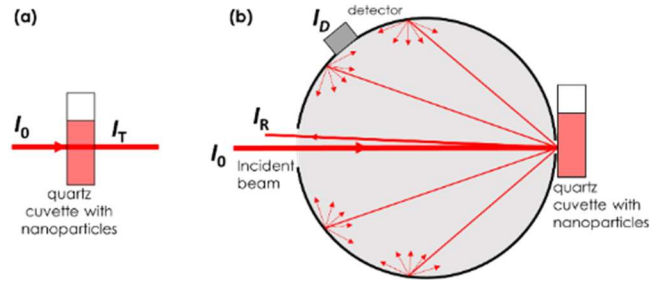

Figure 2. (a) Configuration for transmission measurement (b) Configuration of the integrating sphere for measuring the diffuse reflectance spectra. $I_0$is the illumination light intensity, I_T the transmitted intensity, I_D the diffused intensity and I_R the specular reflected intensity.

Transmission spectra and diffuse reflection spectra were systematically recorded for each of the twelve solutions of the study. Nanoparticle suspension **Au16** was used without further dilution, while all the other samples have been diluted four times (1 ml of AuNPs solution with 3 ml deionized water). Concentrations *C* of the nanoparticles in solution (table 2) were calculated using the method established by W. Haiss[24] and based on a Beer-Lambert law. It states: $C = A_{450}/(\varepsilon_{450} \times d)$ where A_{450} is the experimental values of the absorbance at 450 nm, ε_{450} is the calculated values of the molar extinction coefficient at 450 nm and *d* is the optical path in the cuvette (*d* = 1 cm). The experimental data are given in Table S1.

Numerical calculations

The optical properties of the AuNPs were computed from the Mie theory that allows an exact calculation of the absorption, scattering and extinction cross sections of spheres. Here, we have systematically considered that the AuNPs could be assimilated to perfect nanospheres and we disregarded the optical effects induced by faceted nanoparticles, polycrystalline assemblies or the presence of the molecular surfactant.[25-27] Mie theory was implemented from the PyMieScatt library developed for the Python programming language.[28, 29] We have setup a freely accessible webpage (www.bichromatics.com/calculator) for displaying the results with an interactive interface where the user can adjust several key parameters such as the nanoparticle diameter, the nature of the metal and the surrounding optical index.[30] The calculator uses the optical indices of Johnson and Christy for gold, silver and copper.[31] It includes the option of calculating the cross sections for core-shell spherical nanoparticles, with silica for the core or for the shell. This online calculator allows calculating and plotting several other features that will be discussed in the following.

Results

The twelve AuNPs suspensions were analyzed with a transmission electronic microscope (TEM). The TEM images (Figure 3 and Figure S1) show homogeneous quasi-spherical nanoparticles, with a size varying from 16 to 108 nm. For each TEM image, the size distribution was measured and fitted with a lognormal distribution. Figure 3 shows the case of solutions **Au16**, **Au47**, **Au78** and **Au108** along with their size distribution. The mean diameter, the standard deviation σ, and polydispersity index (PDI = σ / diameter) are given in Table 1. The relatively high size dispersion of the seeds (PDI = 0.11) has no incidence on the polydispersity of the grown AuNPs, since the PDI drops quickly to 0.07 over the growth sequences (Table 1). As already stated in the Bastus' article,[23] this size focusing is indicative of a diffusion-controlled growth mechanism[32].

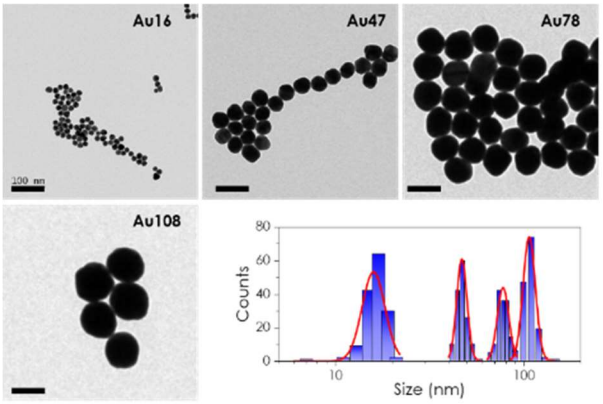

Figure 3. TEM images of the Au NPs **Au16**, **Au47**, **Au78**, **Au108** (scale bar is 100 nm) and size distributions fitted with lognormal distribution. The AuNPs are diameters are 16.7 ± 1.8; 47.0 ± 2.9; 78.1 ± 5.9; and 107.4 ± 6.4 nm respectively.

Published in J. Mater. Chem. C, 2023, 11, 15824
https://doi.org/10.1039/D3TC02669H

Sample	Au16	Au24	Au36	Au44	Au47	Au52	Au60	Au66	Au78	Au85	Au96	Au108
Diameter /nm	16.7	24.7	36.1	43.6	47.0	52.2	60.3	66.4	78.1	85.1	95.2	107.4
σ /nm	1.8	2.4	2.8	2.6	2.9	3.6	4.9	4.3	5.9	6.3	6.4	6.4
PDI	0.11	0.10	0.08	0.06	0.06	0.07	0.08	0.06	0.07	0.07	0.07	0.06

Table 1. Mean diameter, standard deviation and polydispersity index of the Au nanoparticles.

Sample	Au16	Au24	Au36	Au44	Au47	Au52	Au60	Au66	Au78	Au85	Au96	Au108
[AuNPs] / x10^{18} NPs/m^3	0,85	0,20	0,078	0,049	0,042	0,033	0,022	0,017	0,011	0,0085	0,0059	0,0043
C_{calc} /mol/L	1,40 x 10^{-9}	3,37 x 10^{-10}	1,30 x 10^{-10}	8,19 x 10^{-11}	7,02 x 10^{-11}	5,43 x 10^{-11}	3,66 x 10^{-11}	2,86 x 10^{-11}	1,77 x 10^{-11}	1,41 x 10^{-11}	9,73 x 10^{-12}	7,16 x 10^{-12}
Trans – exp	519	521	522	524	526	529	532	535	541	547	554	563
λ_{max} /nm | calc	523	524	526	528	529	531	534	538	546	553	565	579
σ_{ext} calc	523	524	526	528	529	531	534	538	546	553	565	579
Diff R – exp	n.d.[a]	*574*[b]	*576*[b]	574	578	581	585	588	593	597	602	608
λ_{max} /nm | calc	558	553	565	573	579	579	584	589	600	606	620	637
σ_{sca} calc	**530**	**531**	**533**	**536**	**537**	**538**	**542**	**546**	**556**	**564**	**574**	**587**

Table 2. Nanoparticle density in NPs/m^3 and cconcentrations in mol/L of the AuNPs dispersions used in our experiments. Wavelengths of the peak of the LSPR in transmission (measured and calculated) and in diffuse reflectance (measured and calculated). The values of the extinction and scattering cross sections obtained from the Mie theory are also given for the sake of comparison (see discussion). Notice the strong differences between the peak wavelength of the diffuse spectra of the solution, and the scattering spectra of individual nanoparticles (last two lines). ([a]) n.d. is for *non detectable*. ([b]) the signal is very low and noisy making the peak position very uncertain.

UV-visible spectroscopy was performed on diluted solutions (see nanoparticle concentrations in Table 2) in transmission (Figure 4-a) and in diffuse reflection (Figure 4-b) with the integrating sphere. Figure 4-a shows the transmission spectra obtained for the different size of the AuNPs, where the LSPR clearly appears as a pronounced minimum for each sample. This resonance is detected at 519 nm for solution **Au16** and progressively shifts to higher wavelengths as the size increases, reaching 563 nm for **Au108**. All these values are given in Table 2. The diffuse reflectance spectra are represented in Figure 4-b and each spectrum exhibits a clear single peak except for **Au16**, where the scattering is too low to be detected. For **Au24** the maximum is detected at 574 nm and increases to 608 nm for **Au108**. The other values can be found in Table 2.

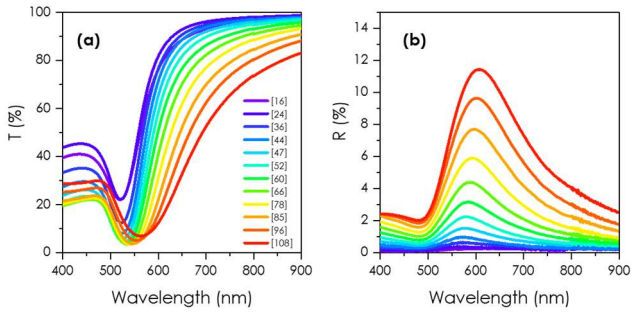

Figure 4. Spectra measured in (a) transmission and (b) diffuse reflection for the twelve AuNPs dispersions. The cuvette was 10 mm thick and the concentrations are indicated in Table 2.

The optical response of one isolated spherical nanoparticle is accurately described by the Mie theory.[33-35] It calculates the three optical cross sections: absorption, extinction and

Published in J. Mater. Chem. C, 2023, 11, 15824
https://doi.org/10.1039/D3TC02669H

scattering. They are represented Figure 5 for gold nanospheres of diameters 24, 52 and 96 nm placed in water with optical index *n* = 1.33 and for all the diameters of interest in Figure S2 of the ESI. This figure shows that the absorption process is dominant over scattering for 24 nm nanoparticles. For 52 nm scattering is not negligible anymore and become dominant for 96 nm. This explains why small particles do not scatter and their colour is dominated by the absorption whose peak is at the LSPR at 524 nm. This absorption of the green wavelength results in the red colour of nanoparticles in this range of size. For particles larger than 50 nm the scattered colour starts being visible, and finally is dominant over absorption. This explains why materials containing such nanoparticles display two different colours in transmission and in diffuse reflection. For example, Figure 5-c shows that for 96 nm AuNPs the peak of the scattering cross section is at 574 nm. This causes the appearance of the biochromatic effect that can be seen on the photographs of Figure 1. However, the peak of the diffuse reflectance was measured at 602 nm and not 574 nm. This difference is not negligible for the perception of colours since 574 nm corresponds to yellow and 602 nm to orange. This discrepancy is shown in Table 2 and it explains why predicting plasmonic colours is specially challenging for materials containing nanoparticles with important scattering efficiency. We will address this aspect in the discussion.

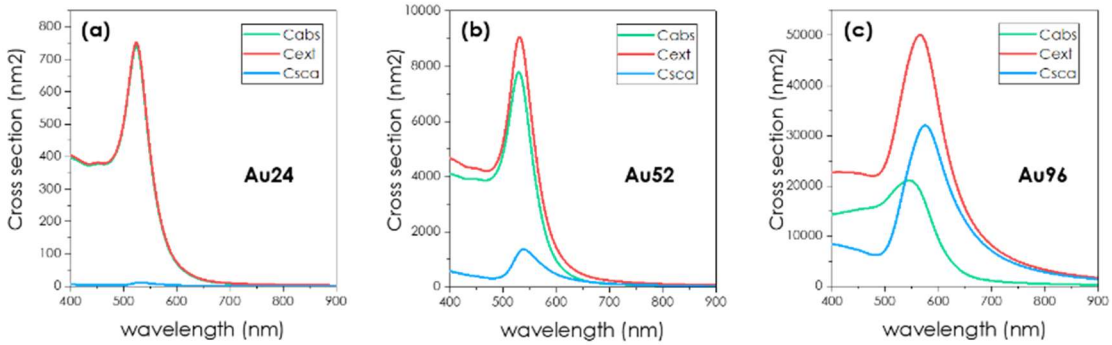

Figure 5. Extinction (red), absorption (green) and scattering (blue) cross-sections spectra for three AuNPs dispersion in water: (a) Au24, (b)/ Au52 and (c) Au96.

Discussion

Calculation of the transmission and diffuse reflectance spectra

The optical cross sections (extinction, absorption and scattering) describe the interaction of a single nanoparticle with a light beam. However, when dealing with an assembly of nanoparticles such as a suspension, or nanoparticles embedded in a solid material, the interaction is more complex, since a light beam can be successively absorbed and scattered, before being detected. Therefore, the calculations of the absorption spectrum and of the diffusion spectra have to be discussed with care.

The transmission spectrum through a suspension of gold nanoparticles such as the spectra of Figure 4-a results from the interaction of light with the assembly of AuNPs dispersed in water. This interaction is properly described by the Beer-Lambert law, where the absorbance *A* writes:

$$A = \varepsilon_{AuNP} \cdot C \cdot d \quad (1)$$

Here, ε_{AuNP} is the molar extinction of the AuNPs, *C* is their concentration and *d* is the optical path inside the cuvette. *A* is related to the transmission *T* that was measured in our experiments with: $A = -\log T = -\log I_T/I_0$. Moreover, ε_{AuNP} can be expressed as a function of the extinction cross section through $\varepsilon_{AuNP} \cdot C \cdot \ln 10 = \sigma_{ext} \cdot n$, where *n* is the density of nanoparticles (number per unit volume). The derivation is detailed in Section 4 of the S.I. Therefore, the transmitted intensity through the assembly of AuNPs writes:

$$I_T = I_0 \exp(-\sigma_{ext} \cdot n \cdot d) \quad (2)$$

Using the particle density from Table 2 and the calculated cross sections shown Figure 5 and Figure S2, all the transmission spectra were computed. The comparison between the computed and experimental spectra for the samples Au24, Au52 and Au96 is shown by the blue curves in Figure 6. There is a remarkable agreement, both in the LSPR position and in the transmitted intensity. These calculations also demonstrate that the minimum in transmission spectra exactly correspond to the plasmon resonance which is indicated by the maximum of the extinction cross section (table 2). Actually, Equation (2) shows that the transmission spectrum depends only on one cross section, the extinction cross sections. This explains why the peak maximum of the extinction cross sections corresponds to the peak maximum of the transmission spectrum.

The computation of the diffuse reflection spectra is more delicate. A light beam that penetrates the nanoparticle suspension is partially absorbed by the nanoparticles on the path (represented by the extinction cross section), until it is back-scattered with an efficiency determined by the scattering extinction. This back-scattering event occurs at a depth *x* inside the solution (see Fig. S3 in the ESI for more details). Then this light beam is reflected and needs to cross again the same solution thickness. Similar backscattering events occur over the full depth of the solution ($0 \leq x \leq d$) and after integrating over

Published in J. Mater. Chem. C, 2023, 11, 15824
https://doi.org/10.1039/D3TC02669H

x, it yields the following relationship for the back-diffused intensity:

$$I_{Diff} = \frac{1}{2}\beta I_0 \frac{\sigma_{sca}}{\sigma_{ext}}[1 - \exp(-2\sigma_{ext} \cdot n \cdot d)] \quad (3)$$

In Equation (3) the coefficient β takes into account the fact that for establishing this simple formula only the exact back-scattering was considered whereas our spectrometer integrates over all the directions. From the Mie theory, it is known that the scattering is maximum for back-scattering. Therefore Equation (3) is expected to overestimate the quantity I_{Diff} and using $\beta = 0.2$ provides a correct result. In order to present an analytical equation, that remains easy to use, we did not include these angle dependent cross sections. The spectra calculated with Equation (3) are given in Figure 6 and are compared with the experimental data (red curves). The agreement is excellent in term of LSPR peak position and in term of intensity. For example, for **Au52**, the peak position is measured at 581 nm and is calculated at 579 nm. Notice also that the maximum of the scattering cross section was at 538 nm, strongly under-estimated compared to the measured value. This shows clearly that the peak wavelength of the diffused light does not match the LSPR. This result is important because it explains why the colours in transmission and in diffusion are not exactly complementary colours. These results also stress the strong variation of the diffused intensity when the nanoparticle diameter increases: it was 0.4 % for **Au24**, 2.3% for **Au52** and about 9 % for **Au96**. The complete simulations for all twelve solutions are presented in Figure S4 of the ESI.

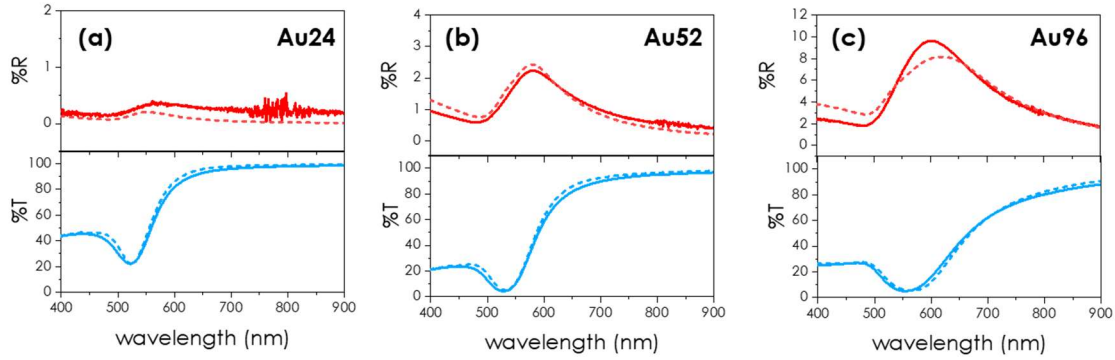

Figure 6. Experimental (line) and calculated (dash line) spectra for the transmitted (blue) and back-scattered (red) light for three AuNPs dispersions: (a) **Au24**, (b) **Au52** and (c) **Au96**. The diffused intensity is very low for **Au24** which is the cause of the noise detected at 800 nm.

Furthermore, the wavelengths of the minimum in the transmission spectra and of the maximum in the diffuse reflectance spectra are shown in Table 2 and displayed Figure 7, for both the calculated and the measured values. The error bars are also indicated. They have different origins depending on the spectra, and they are linked to the uncertainty in determining the position of the maximum for very broad peaks, or to the high level of noise for some spectra. The prediction of the transmission minimum is very accurate for nanoparticles of diameters between 16 and 85 nm. However, the error is of 16 nm for **Au108**. Nevertheless, the overall shapes of the spectra are very well reproduced, which is essential if the goal is to be able to predict the colour of such a plasmonic material. Regarding the diffuse reflectance spectra, the position of the maximum is exact (within error bars) from 24 nm to 80 nm (Figure 7). This agreement contrasts sharply with most published data where the diffusion spectra of nanoparticles was analyzed by discussing the scattering cross sections. Curve (e) in Figure 7 illustrates the strong discrepancy between the peak position of σ_{sca} and the peak of the diffuse reflectance spectra. σ_{sca} gives a systematic underestimation of 40 nm. Some authors have extracted the ratio $\sigma_{sca}/\sigma_{abs}$ from diffusion measurements and stressed the good agreement between experiments and calculations.[36] Actually, our Equation (3) confirms that the spectra should be proportional to $\sigma_{sca}/\sigma_{abs}$. Equations (2) and (3) have been implemented on the online calculator which allows a rapid estimation of the spectra of the most common plasmonic metals.[30]

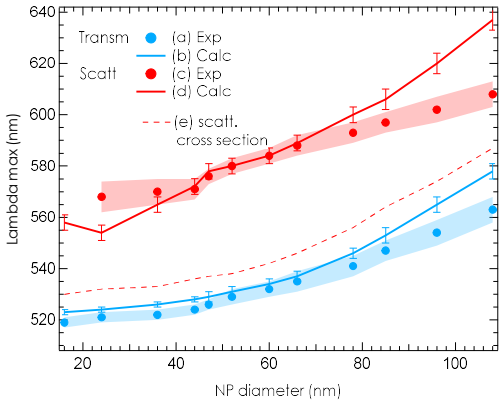

Figure 7. Experimental (filled circles) and simulated (line) wavelengths of the LSPR peak for the transmitted (blue) and back-scattered (red) light as a function of the nanoparticle size. Error bars are also given. The thin dotted line (e) corresponds to the calculated scattering cross section.

Published in J. Mater. Chem. C, 2023, 11, 15824
https://doi.org/10.1039/D3TC02669H

Colour calculations in transmission and in reflection

Now that we have established how to calculate realistic spectra for the transmission and the diffusion of our plasmonic particle suspensions, it is possible to predict the colours of this material and compare them with the reality. Colour is not a property of the electromagnetic wave transmitted or diffused by an object but a subjective perception of an observer. The human eyes perceive colours with its three types of cone cells. These cone cells have their peak sensitivity for three colours, blue green and red. This is the fundament of the tristimulus method, that was established into a scientific and quantitative description by the CIE (*Commission Internationale de l'Eclairage*) in 1931. Finally, a colour is characterized by three parameters: its *hue* (blue, yellow, orange, etc), its *saturation* (a vivid red *vs*. a dull red) and its *brightness*.[37] The CIE 1931 colour chromaticity diagram (see Figure 8) is a way of representing in 2D the hue and the saturation of colours with Cartesian coordinates (x,y). However, the brightness appears as a third dimension and cannot be plotted easily. Therefore, it is often set to an average value. This could alter the colour rendering. Colour calculation is summarized for example in the following references. [5, 12]

The transmitted and the diffused colours of our twelve AuNPs solutions have been represented in the CIE 1931 chromaticity diagram in Figure 8. For each solution, the colour coordinates were obtained by processing the transmission spectra (squares marked T16 to T108 on Figure 8) and the diffuse reflectance spectra (filled circles D16 to D108 in Figure 8). Here the illuminant D65 was used for simulating the classical daylight source. The calculations have been implemented in our online calculator[30] and the colours are given in various coordinate systems: XYZ, *L*a*b**, L*C*h*. The resulting colour is represented in RGB colours on the webpage and gives an idea of the colour of the corresponding plasmonic material. [30] More details and a screenshot of the web interface are shown in in Figure S5 of the ESI.

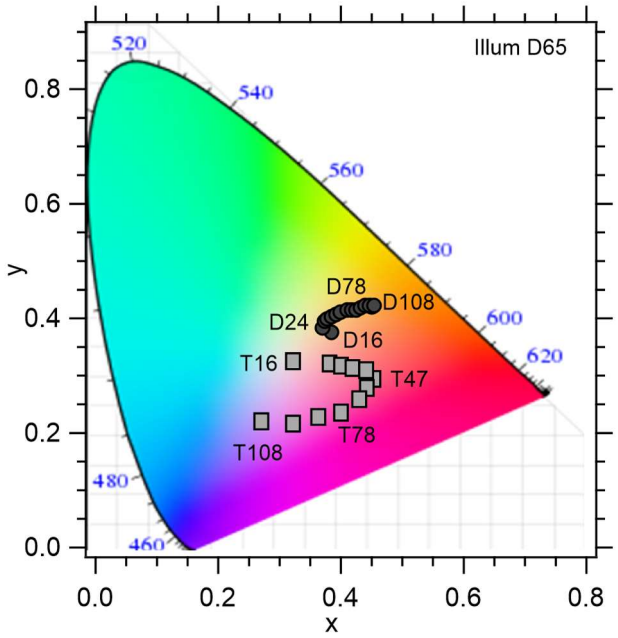

Figure 8. Representation in the CIE colour diagram of the colours of 12 AuNPs solutions with increasing diameters from 16 to 108 nm. D16 to D108 (circles) correspond to the colours in diffusion and T16 to T018 (squares) to the transmitted colours. Illuminant is the D65 daylight.

Figure 8 shows that in transmission, our solution **Au16** is seen as a dull red and when increasing the nanoparticle size, the solution goes to a nice and strong red for **Au47**, then takes a purple and violet colouration for larger diameters. However, this colouration depends strongly on the nanoparticle density (or material thickness) and on the surrounding index. The online calculator allows exploring very quickly the possible colours perceived by the human eyes. In order to check the accuracy of the colour calculations, the results are shown in Figure 9 for five solutions. The comparison of an RGB rendering of Figure 9 with the photographs of Figure 1 is very approximate due to the multiple processes for displaying colour images. However, the appearance looks very similar.

Regarding the diffusion, the situation is more complex also. Figure 8 shows the variation of colours with the increasing nanoparticle diameter, denoted D16 to D108. The colour starts from a light brown at D16 to a more saturated orange when the diameter grows larger than 80 nm. However, as mentioned above, the diffusion efficiency is below 1 % for diameters smaller than 45 nm (see Figure S4). It means that no more than 1% of the incident light is back-scattered. Subsequently, the colour in diffusion will hardly be noticed in usual environments. For materials with larger AuNPs, such as **Au52**, the diffusion efficiency is 2.4 % at the peak wavelength. If this object is small in size, its colour will certainly be drowned out by the surrounding objects. However, if the object is large enough, or if it is selectively illuminated, then the diffusion colour will be easily observed. This could give rise to very nice and intriguing visual effects. For **Au52**, the colour is represented in Figure 9 and is light brown. In the representation of Figure 9-c, when the diffusion efficiency was too low, we have applied an amplification coefficient between 1 and 20 in order to consider

Published in J. Mater. Chem. C, 2023, 11, 15824
https://doi.org/10.1039/D3TC02669H

the fact that the eyes of an observer spontaneously adjust their sensitivity. This coefficient is related to the β coefficient in Equation (3). When $\beta = 0.2$, there is no amplification. For example for **Au16**, even with the 20 times amplification ($\beta = 4$), the total efficiency remained at 1.5% and subsequently the diffused colour is a very dark green that appears black. For **Au78**, $\beta = 1.9$ which corresponds to an amplification of 14 and the color is predicted to be light beige and with a diffused intensity that is 80 % of the incoming energy. This means that this color is easily perceived by the observer. This is confirmed by the photograph of Figure 1-b where the brown-orange color of **Au78** is obvious.

Figure 9 also compares the colours predicted by our models with the colour measured with our spectrometer for five diameters of AuNPs. Transmission is presented in Figure 9-a) and b) for measures and calculations respectively. The hues are fairly accurate and even if for **Au108**, the calculated and the measured hues tends to differs slightly. Regarding the diffused colours presented in Figure 9-c) and d), the agreement is more approximate which is due to our limited hypothesis used for deriving Equation (3) where only the 180° back-scattering is included. The full colour coordinates in several systems (L*a*b*, L*C*H* and RGB) are given in Tables S2 and S3 of the ESI. Figure 9 shows that our approach with Equation (2) and (3) provide a very efficient way for predicting the colouring power of plasmonic pigments when AuNPs are embedded in a material.

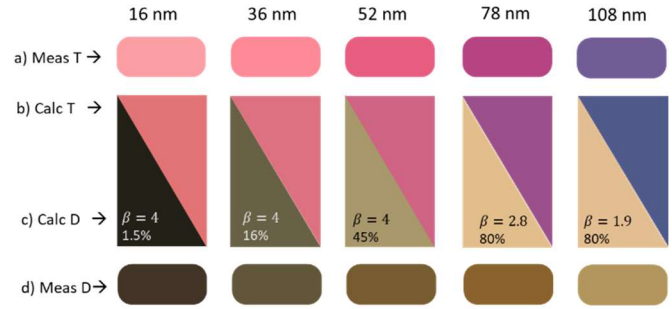

Figure 9. Illustration of the bichromatic effect for nanoparticles larger than 50 nm where the colours perceived in transmission and in diffusion for five samples are represented. The experimental transmitted colours (a) are compared to the calculated transmitted colours (b). Similarly, the colours in diffusion are represented for the measured solutions (c) and the calculations (d). The luminance of the reflected light was amplified by a factor of 20 ($\beta = 2.8$) for samples **Au16**, **Au36** and **Au52** and by a factor of 14 for **Au78** ($\beta = 4$) and 9.5 for **Au108** ($\beta = 1.9$). The percentage indicates the resulting ratio of the back-scattered intensity to the incoming intensity.

The bichromatic effect

For gold nanoparticles of diameters greater than 70 nm, the scattering cross section becomes comparable to the absorption cross section as explained above. Therefore, the colour diffused by the material becomes perceptible. Roughly, one can understand that the colour in diffusion will be dominated by the peak wavelength in scattering: 560 nm (yellow/green) for 70 nm AuNP. On the other hand, the colour in transmission is defined by the maximum of the extinction: 540 nm (green) for 70 nm. This colour will be missing in the perceived colour and the complementary colour will be observed (purple in our example). This perception of roughly two complementary colours, purple in transmission and green in diffusion, is the *bichromatic* effect, observed in the Lycurgus cup. [7,8] As detailed above, the two colors are not exactly complementary, since the minimum wavelength of transmission does not match the peak wavelength of diffusion. Notice that some authors talk about dichroic effect, but rigorously speaking *dichroism* refers to a material that absorbs light differently in two different conditions such as two different polarizations or two different angles of incidence. Here, the difference is whether absorption or scattering is favored. *Bichromatism* seems more appropriate. As discussed above and shown in Equation (3), the colour in diffusion is a combination between scattering and extinction. The consequence is that the peak tends to flatten slightly and the saturation of the colour decreases. As shown in Figure 9 the variation of colour in diffusion is rather limited and remain light brown and hardly reach the orange colour. Our results show that the diffused colour will never be a vivid colour. Nevertheless, the dual colourations that were detected in the photographs of Figure 1 are nicely reproduced. Figure 9 demonstrates that for particles smaller than 50 nm the diffused intensity is very low (1.5 % for **Au16** and 16 % for **Au36**) and this material will not exhibit any detectable *bichromatic* effect. This is confirmed by photographs of Figure 1. The *bichromatic* effect could certainly be used to generate unexpected perceptions based on plasmonic pigments in paintings, coatings or inks because the behaviour is very different from conventional pigments. The bichromatic effect will appear especially intriguing if bichromatic printed area are placed next to an area with usual ink. The contrast will change when the illumination will be changed. Applications can be envisioned in design and anticounterfeiting.

Conclusions

In this study we have systematically explored the optical properties of spherical nanoparticles in water, when their diameter is increased from 16 nm to 108 nm. We have prepared twelve different sample solutions with increasing nanoparticle diameters and measured the spectra in transmission and in diffuse reflectance. These experiments clearly show the progressive uptake of the *bichromatic effect* when nanoparticles are greater than 70 nm. It shows up as the perception of two different colours in diffusion and in transmission, depending if the source of light and the observer are respectively on the same side, or on the opposite sides relatively to the sample. The two colours are almost complementary colours but not exactly. These effects were discussed using a simple analytical model based on the cross sections from the Mie theory and the model was implemented on a freely accessible online calculator, where the spectra and the colours are calculated. This study demonstrates that spherical gold nanoparticles in water exhibit a variation of colours from pink, red, purple to violet in transmission when their size increases. In diffusion, the colour remains beige and brown with a relatively low saturation. We limited this study to spherical nanoparticles to make the confrontation between

simulations and experiments more convincing. However, our results could be easily extended to other plasmonic nanoparticles, with other shapes or other materials. This opens new possibilities for using plasmonic pigments and generate intriguing visual effects.

Conflicts of interest

There are no conflicts to declare.

Acknowledgements

The authors are grateful to A. Lehoux, D. Schaming and H. Remita for initial discussions and work about the colours of gold nanoparticles. OP and WW acknowledge a financial support from the SATT Lutech for the *Bichromatics* project in 2017.

Notes and references

1. C. S. Kealley, M. B. Cortie, A. I. Maaroof and X. Xu, Phys. Chem. Chem. Phys., 2009, 11, 5897-5902.
2. O. Pluchery, H. Remita and D. Schaming, Gold Bulletin, 2013, 46, 1-9.
3. P. K. Jain, K. S. Lee, I. H. El-Sayed and M. A. El-Sayed, The Journal of Physical Chemistry B, 2006, 110, 7238-7248.
4. O. Pluchery and J.-F. Bryche, An Introduction to plasmonics, World Scientific Publishing, London, 2023.
5. M. Song, D. Wang, S. Peana, S. Choudhury, P. Nyga, Z. A. Kudyshev, H. Yu, A. Boltasseva, V. M. Shalaev and A. V. Kildishev, Applied Physics Reviews, 2019, 6, 041308.
6. F. Dekker, L. Kool, A. Bunschoten, A. H. Velders and V. Saggiomo, Chemistry Teacher International, 2021, 3.
7. D. J. Barber and I. C. Freestone, Archaeometry, 1990, 32, 33-45.
8. I. Freestone, N. Meeks, M. Sax and C. Higgitt, Gold Bulletin, 2007, 40, 270-277.
9. P. N. Njoki, I. I. S. Lim, D. Mott, H. Y. Park, B. Khan, S. Mishra, R. Sujakumar, J. Luo and C. J. Zhong, Journal of Physical Chemistry C, 2007, 111, 14664-14669.
10. C. Noguez, The Journal of Physical Chemistry C, 2007, 111, 3806-3819.
11. E. A. Coronado, E. R. Encina and F. D. Stefani, Nanoscale, 2011, 3, 4042.
12. O. Aftenieva, D. Schletz, A. Meyer, T. Kuhne, S. Schmalzriedt, M. Niethammer and T. A. F. Konig, Journal of Chemical Education, 2021, 98, 2566-2573.
13. M. Blosi, S. Albonetti, F. Gatti, G. Baldi and M. Dondi, Dyes and Pigments, 2012, 94, 355-362.
14. C. Gautier, A. Cunningham, L. Si-Ahmed, G. Robert and T. Bürgi, Gold Bulletin, 2010, 43, 94-104.
15. J. D. Smith, M. A. Reza, N. L. Smith, J. Gu, M. Ibrar, D. J. Crandall and S. E. Skrabalak, ACS Nano, 2021, 15, 2901-2910.
16. X. F. Gao, Q. Wang, S. J. Zhang, R. J. Hong and D. W. Zhang, Optics Communications, 2022, 517.
17. J. Peng, H.-H. Jeong, M. Smith, R. Chikkaraddy, Q. Lin, H.-L. Liang, M. F. L. De Volder, S. Vignolini, S. Kar-Narayan and J. J. Baumberg, Advanced Science, 2021, 8, 2002419.
18. W. H. Yang, S. M. Xiao, Q. H. Song, Y. L. Liu, Y. K. Wu, S. Wang, J. Yu, J. C. Han and D. P. Tsai, Nature Com., 2020, 11.
19. F. Neubrech, X. Duan and N. Liu, Science Advances, 2020, 6, eabc2709.
20. Europe Pat., 2017.
21. A. S. Roberts, A. Pors, O. Albrektsen and S. I. Bozhevolnyi, Nano Lett., 2014, 14, 783-787.
22. G. Frens, Nature-Physical Science, 1973, 241, 20-22.
23. N. G. Bastus, J. Comenge and V. Puntes, Langmuir, 2011, 27, 11098-11105.
24. W. Haiss, N. T. K. Thanh, J. Aveyard and D. G. Fernig, Analytical Chemistry, 2007, 79, 4215-4221.
25. M. Hu, C. Novo, A. Funston, H. Wang, H. Staleva, S. Zou, P. Mulvaney, Y. Xia and G. V. Hartland, Journal of materials chemistry, 2008, 18, 1949-1960.
26. A. Movsesyan, S. Marguet, A. Muravitskaya, J. Béal, P.-M. Adam and A.-L. Baudrion, J. Opt. Soc. Am. A, 2019, 36, C78-C84.
27. U. Mansfeld, F. Pellegrino, V. Maurino, S. Marguet, F. Testard, O. Tache and V.-D. Hodoroaba, Microscopy and Microanalysis, 2019, 25, 2328-2329.
28. B. J. Sumlin, W. R. Heinson and R. K. Chakrabarty, Journal of Quantitative Spectroscopy and Radiative Transfer, 2018, 205, 127-134.
29. B. Sumlin, PyMieScatt, https://pymiescatt.readthedocs.io/en/latest/index.html).
30. W. L. Watkins and O. Pluchery, Bichromatics, spectrum calculator, www.bichromatics.com/calculator/, 2020).
31. P. B. Johnson and R. W. Christy, Physical Review B, 1972, 6, 4370.
32. N. T. K. Thanh, N. Maclean and S. Mahiddine, Chem. Rev., 2014, 114, 7610-7630.
33. C. F. Bohren and D. R. Huffman, Absorption and Scattering of Light by Small Particles., Wiley-Interscience, New-York 1998.
34. K. L. Kelly, E. Coronado, L. L. Zhao and G. C. Schatz, J. Phys. Chem. B, 2003, 107, 668-677.
35. D. Tzarouchis and A. Sihvola, Appl. Sci, 2018, 8, 184.
36. E. G. Wrigglesworth and J. H. Johnston, Nanoscale Advances, 2021, 3, 3530-3536.
37. R. Sève, Science de la couleur, Chalagam Edition, 2009.